Supporting Information for:

Polynuclear Cu_4L_4 copper(II)-aminyl radical coordination complexes.

Nico M. Bonanno,[a] Alan J. Lough,[b] and Martin T. Lemaire*[a]

[a]*Department of Chemistry, Brock University, St. Catharines, Ontario, L2S 3A1, Canada.*
[b]*Department of Chemistry, University of Toronto, Toronto, Ontario, M5S 3H6, Canada.*

*Corresponding author e-mail: mlemaire@brocku.ca

Table of Contents

General considerations. **S2**
Scheme S1. Synthesis of MeH_3L (**5**). **S2**
Synthesis. **S2**
Computational details. **S5**
References. **S5**
Table S1: Crystal data for **1.** **S7**
Table S2: Crystal data for **2.** **S8**
Table S3. Relevant bond distances (Å) and angles (°) for **1**. **S9**
Table S4. Relevant bond distances (Å) and angles (°) for **2**. **S13**
Figure S1. Molecular structure of **2**. **S17**
Figure S2. View of the molecular structure of **2.** **S18**
Figure S3. View of the Cu_4O_4 core in **2**. **S19**
Figure S4. ^1H NMR spectrum of **4** in $CDCl_3$. **S20**
Figure S5. ^{13}C NMR spectrum of **4** in $CDCl_3$. **S21**
Figure S6. ESI mass spectrum of **1.** **S22**
Figure S7. ESI mass spectrum of **2.** **S23**
Figure S8. Comparison of the FT-IR spectra of powder and crystal samples of **1**. **S24**
Figure S9. Comparison of the UV-visible spectra of powder and single crystal **1.** **S24**
Figure S10. Experimental pXRD spectrum of complex **1**. **S25**
Figure S11. Calculated pXRD spectrum from the single crystal X-ray structure of **1.** **S25**
Figure S12. Experimental pXRD spectrum of complex **2**. **S26**
Figure S13. Calculated pXRD spectrum from the single crystal X-ray structure of **2.** **S26**
Figure S14. UV-visible-NIR spectrum of **1**. **S27**
Figure S15. Magnetic exchange coupling model for **1** and **2**. **S28**
Figure S16. Variable temperature magnetic susceptibility data for **2**. **S28**
Figure S17. Mulliken spin densities in the unrestricted singlet state of complex **1**. **S30**
Table S6. Mulliken spin densities of selected atoms in complex **2**. **S30**
Figure S18. Mulliken spin densities in the unrestricted singlet state of complex **2**. **S31**
Table S6. Mulliken spin densities of selected atoms in complex **2**. **S31**

General considerations

All reagents were commercially available and used as received unless otherwise stated. Anhydrous solvents (MeOH, THF, toluene) were obtained by distillation over CaH_2 or obtained from a PureSolve solvent purification system. FT-IR spectra were recorded with a Shimadzu IRAffinity spectrometer as KBr discs. UV-Vis measurements were recorded with a Shimadzu 3600 UV-Vis-NIR spectrophotometer in THF solution using quartz cuvettes. High resolution EI mass spectra were acquired with a Thermo Scientific DFS (Double Focusing Sector) mass spectrometer. ESI mass spectra were obtained with a Bruker HCT Plus ion-trap by direct infusion of the sample using a syringe pump. $^1H/^{13}C$ NMR spectra were obtained with a Bruker Avance AV 400 Digital NMR spectrometer with a 9.4 Tesla Ascend magnet in $CDCl_3$. Microanalyses were performed by Canadian Microanalytical Ltd, Delta, BC, Canada. Variable temperature magnetic susceptibility measurements for **1** and **2** were obtained with an QD-MPMS SQUID magnetometer at an external magnetic field of 5000 Oe over a temperature range of 5-325K. Corrections for the diamagnetism of the sample holder were made by subtracting the straw and empty gel cap data from the experimental emu values and diamagnetic corrections for atoms and bonds were calculated using Pascal's constants.

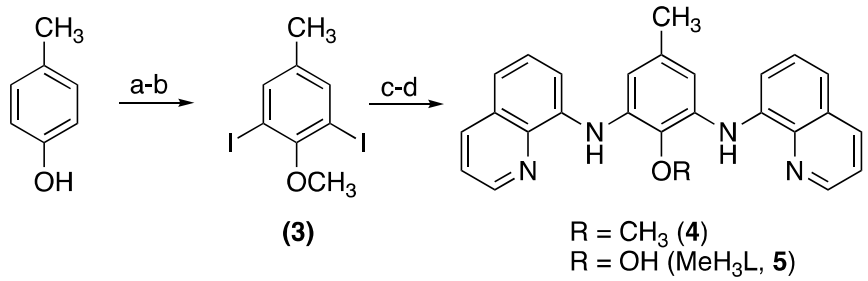

Scheme S1. Synthesis of MeH_3L (**5**). Reagents and conditions: (a) KI/30% H_2O_2 (conc H_2SO_4/MeOH), (b) MeI/K_2CO_3 (Acetone, reflux), (c) 8-aminoquinoline/$Pd(OAc)_2$/BINAP/Cs_2CO_3 (toluene, reflux), (d) BBr_3 (1 M, DCM)

Synthesis

1,3-Diiodo-2-methoxy-5-methylbenzene (3). To a round-bottom flask containing MeOH (600 mL) and concentrated H_2SO_4 (14 mL) was added 4-methylphenol (14.5 g, 134 mmol) and KI (44.5 g, 268 mmol). An aqueous solution of H_2O_2 (30%, 50 mL) was added and the reaction mixture was stirred overnight at 40°C and then was let cool to room temperature. The reaction contents were diluted with CH_2Cl_2 and washed with $NaHSO_3$ (0.1 M) and H_2O. The organic layer was evaporated to dryness and then dissolved in 500 mL of acetone in a round bottom flask equipped with a magnetic stir bar. Iodomethane (8.3 mL, 134 mmol) and K_2CO_3 (37.0 g, 268 mmol) were added. The reaction mixture was refluxed for 12 h, cooled to room temperature and diluted with CH_2Cl_2 and then washed with water. The aqueous layer was separated and extracted twice with CH_2Cl_2. The combined organic fractions were pre-absorbed on silica gel and the compound was purified by flash chromatography using either petroleum ether or hexanes and by collecting the first product to come off of the column, resulting in a colorless oil. Yield, 16.8 g (33.4 %). ^{1}H NMR (400 MHz, $CDCl_3$): δ 7.60 (s, 2H), 3.85 (s, 3H), 2.26 ppm (s, 3H). MS (ESI, +): 396.8 ($[M+Na]^+$, 100%).

2-Methoxy-1,3-*bis*(8-quinolylamino)-5-methylbenzene (4). A Schlenk flask containing anhydrous toluene (150 mL) was loaded with palladium acetate (0.19 g, 5 mol %, 0.86 mmol), BINAP (1.05 g, 1.71 mmol) and heated to approximately 80-90°C and held at this temperature until the solution turned a dark red color. Next, **3** (6.0 g, 16 mmol) was added causing the solution color to lighten significantly and this solution was left to stir for an additional 10-15 min. Cs_2CO_3 (20.9 g, 64.0 mmol) was added and the solution was stirred for 10 min and this was followed by the addition of 8-aminoquinoline (4.61 g, 32.0 mmol). The reaction mixture was refluxed with vigorous stirring for 3-5 d and monitored by TLC (1:1 hexanes/DCM) until near complete consumption of starting material was noted. The completed reaction was cooled to RT, diluted with 350 mL of DCM and washed with H_2O. The organic layers were combined, concentrated and pre-absorbed on silica gel. The product was purified by chromatography using first 1:1 hexanes/DCM and then by slowly increasing the proportion of DCM. The first yellow band was identified as a mono-substituted product, the second yellow band was the desired product, which was

concentrated to a bright yellow oil that solidified to a yellow crusty solid after drying under vacuum. Yield, 4.35 g (67%). ^{1}H NMR (400 MHz, $CDCl_3$): δ 8.87 (dd, 2H, *J* = 4, 2 Hz), 8.73 (s, 2H), 8.15 (dd, 2H, *J* = 8, 2 Hz), 7.63 (d, 2H, *J* = 8 Hz), 7.51 (d, 2H, *J* = 8 Hz), 7.48-7.44 (m, 2H), 7.28 (d, 2H, *J* = 8 Hz), 7.20 s (2H), 3.89 (s, 3H), 2.40 ppm (s, 3H). ^{13}C NMR (100 MHz, $CDCl_3$): δ 147.6, 140.0, 139.7, 139.2, 136.1, 135.6, 133.9, 128.9, 127.3, 121.6, 116.7, 112.3, 108.7, 60.3, 22.0 ppm. MS (ESI, +): *m/z* 406 [(M-H)+, 100%]. HRMS (EI+), Calcd for (found) $C_{25}H_{22}N_4O$: 406.1780 (406.1788). FT-IR (KBr, cm^{-1}): 3389 (m), 3345 (m), 3049 (w), 2954 (w), 2924 (m), 2853 (m), 1591 (s), 1572 (s), 1510 (s), 1497(s), 1477 (s), 1458 (m), 1422 (m), 1379 (s), 1331 (s), 1252 (m), 1234 (w), 1217 (m), 1107 (w), 1037 (w), 986 (m), 820 (m), 789 (m), 758 (m), 748 (m), 640 (w), 577 (w).

2,6-Bis(8-quinolylamino)-4-methylphenol (MeH_3L, 5). A Schlenk flask containing anhydrous dichloromethane (150 mL) was cooled to 0°C in ice-water and loaded with **4** (2.5 g, 6.2 mmol). To the cooled solution of **4**, BBr_3 solution (1M, DCM, 14 mL, 14 mmol) was added dropwise. The reaction mixture was left in the ice-water bath and allowed to warm to room temperature overnight. Deoxygenated water (150 mL) was added and the mixture was stirred vigorously for approximately 3-4 hours and then separated. The organic layer was concentrated to a bright orange powder. Yield, 2.1 g (87%). **5** is air sensitive and should be stored in a glove box. We could not obtain NMR data for **5** because it undergoes oxidation in solution to a paramagnetic species. HRMS (EI+): Calcd for (found) $C_{25}H_{20}N_4O$: 392.1632 (392.1614). FT-IR (KBr, cm^{-1}): 3346 (br, m), 3039 (w), 2920 (w), 2853 (w), 1593 (m), 1572 (s), 1514 (s), 1497 (s), 1472 (s), 1422 (m), 1377 (s), 1331 (m), 1215 (w), 1169 (w), 1105 (w), 984 (w), 818 (m), 789 (m), 747 (m), 581 (w).

(^{t}BuL)$_4$Cu$_4$ (1). In a nitrogen-filled glovebox, (98.0 mg, 226 mmol) of ^{t}BuH$_3$L was placed in a 25 mL Erlenmeyer flask equipped with a magnetic stir bar, dissolved in approximately 15 mL of deoxygenated MeOH and left to stir for several minutes. An excess of deoxygenated triethylamine was added (0.75 - 1.0 mL) to the solution of the ligand, which changed from a brilliant orange to a yellowish-brown color. After approximately 20 min, a MeOH solution (2 mL) of $Cu(ClO_4)_2{\cdot}6H_2O$ (78.0 mg, 215 mmol) was added in one portion to the ligand

solution and a dark red color was immediately produced followed by the precipitation of a maroon solid. The solution was stirred overnight, gravity filtered and washed with MeOH (3 x 20 mL). The filtered precipitate was left to dry over several hours. Yield, 81 mg (71%). Calc'd for (found %) $Cu_4C_{112}H_{92}N_{16}O_4{\cdot}4CH_3OH$, C: 66.08 (65.88), H: 5.16 (4.88), N: 10.63 (10.64%). MS (ESI+): *m/z* 1982.3 $[M+H]^+$. FT-IR (KBr, cm^{-1}): 3445 (br, w), 3046 (w), 2959 (m), 1564 (m), 1497 (m), 1466 (s), 1425 (w), 1379 (m), 1333 (w), 1277 (m), 1232 (w), 1198 (w), 1128 (w), 1015 (w), 955 (w), 816 (w), 783 (w), 729 (w), 648 (w), 588 (w). UV-Vis (THF): λ_{max} nm (ε, $M^{-1}cm^{-1}$): 523 (4×10^3). Single crystals were grown in a glove box by dissolving approximately 10 mg of **1** in THF (2 mL). This solution was filtered into a small vial, approximately 1mL of toluene was carefully layered on top of the THF and the vial was capped tightly. After several days the two solvent layers had mixed completely and then the screw cap on the vial was loosened. Purple crystals of **1** deposited on the sides of the vial during the slow evaporation of the solvents.

$(MeL)_4Cu_4$ (2). In an identical similar procedure, complex **2** was prepared from **5** (110 mg, 280 mmol) and (98.6 mg, 266 mmol) of $Cu(ClO_4)_2{\cdot}6H_2O$. Yield, 102 mg (80%). Single crystals of **2** were grown by the same procedure used to grow crystals of **1**. Calc'd for (found %) $Cu_4C_{100}H_{68}N_{16}O_4{\cdot}2CH_3OH{\cdot}5H_2O$, C: 62.31 (61.67), H: 4.41 (3.77), N: 11.40 (11.26%). MS (ESI+): *m/z* 1814.3 $[M+4H]^+$. FT-IR (KBr, cm^{-1}): 3352 (br w), 3044 (w), 2913 (w), 2855 (w), 1562 (s), 1497(s), 1470 (s), 1377 (s), 1331 (m), 1290 (w), 1231 (w), 1211 (w), 1125 (w), 1090 (w), 1018 (w), 984 (w), 785 (m), 741 (m), 671 (w), 636 (w), 588 (w). UV-Vis (THF): λ_{max} nm: 517.

Computational details. Single point energy calculations were performed using the X-ray structure coordinates for **1** and **2** using the B3LYP[1,2] hybrid functional and the def2-SVP basis set on all atoms with the Gaussian09 (Revision D.01)[3] package. Tight SCF convergence criteria were used for all calculations. The program Chemissian[4] was used for the preparation of the spin density distribution figures.

References

[1] Becke, A. D. Density-functional thermochemistry. III. The role of exact exchange. *J. Chem. Phys.* **1993**, *98*, 5648.

[2] Lee, C.; Yang, W.; Parr, R. G. Development of the Colle-Salvetti correlation-energy formula into a functional of the electron density. *Phys. Rev. B* **1988**, *37*, 785.

[3] Gaussian 09, Revision **D.01**, Frisch, M. J.; Trucks, G. W.; Schlegel, H. B.; Scuseria, G. E.; Robb, M. A.; Cheeseman, J. R.; Scalmani, G.; Barone, V.; Mennucci, B.; Petersson, G. A.; Nakatsuji, H.; Caricato, M.; Li, X.; Hratchian, H. P.; Izmaylov, A. F.; Bloino, J.; Zheng, G.; Sonnenberg, J. L.; Hada, M.; Ehara, M.; Toyota, K.; Fukuda, R.; Hasegawa, J.; Ishida, M.; Nakajima, T.; Honda, Y.; Kitao, O.; Nakai, H.; Vreven, T.; Montgomery, J. A., Jr.; Peralta, J. E.; Ogliaro, F.; Bearpark, M.; Heyd, J. J.; Brothers, E.; Kudin, K. N.; Staroverov, V. N.; Kobayashi, R.; Normand, J.; Raghavachari, K.; Rendell, A.; Burant, J. C.; Iyengar, S. S.; Tomasi, J.; Cossi, M.; Rega, N.; Millam, J. M.; Klene, M.; Knox, J. E.; Cross, J. B.; Bakken, V.; Adamo, C.; Jaramillo, J.; Gomperts, R.; Stratmann, R. E.; Yazyev, O.; Austin, A. J.; Cammi, R.; Pomelli, C.; Ochterski, J. W.; Martin, R. L.; Morokuma, K.; Zakrzewski, V. G.; Voth, G. A.; Salvador, P.; Dannenberg, J. J.; Dapprich, S.; Daniels, A. D.; Farkas, Ö.; Foresman, J. B.; Ortiz, J. V.; Cioslowski, J.; Fox, D. J. Gaussian, Inc., Wallingford CT, 2009.

[4] Skripnikov, L. V. *Chemissian* V. 4.01, Visualization Computer Program, www.chemissian.com, 2014.

Table S1: Crystal data for **1.**

Empirical formula	$C_{253}H_{224}Cu_8N_{32}O_{10}$	
Formula weight	4380.95	
Temperature	150(2) K	
Wavelength	1.54178 Å	
Crystal system	Monoclinic	
Space group	$P2_1/n$	
Unit cell dimensions	a = 15.6589(5) Å	α = 90°
	b = 23.3867(8) Å	β = 101.339(3)°
	c = 30.4865(11) Å	γ = 90°
Volume	10946.5(7) $Å^3$	
Z	2	
Density (calculated)	1.329 Mg/m^3	
Absorption coefficient	1.374 mm^{-1}	
F(000)	4556	
Crystal size	0.120 x 0.030 x 0.030 mm^3	
Theta range for data collection	2.399 to 67.228°.	
Index ranges	-18<=h<=17, -27<=k<=22, -35<=l<=34	
Reflections collected	84008	
Independent reflections	19135 [R(int) = 0.1205]	
Completeness to theta = 67.228°	97.6 %	
Absorption correction	Semi-empirical from equivalents	
Max. and min. transmission	0.7529 and 0.6429	
Refinement method	Full-matrix least-squares on F^2	
Data / restraints / parameters	19135 / 3 / 1325	
Goodness-of-fit on F^2	1.024	
Final R indices [I>2sigma(I)]	R1 = 0.0694, wR2 = 0.1685	

R indices (all data)	R1 = 0.1345, wR2 = 0.2048
Extinction coefficient	0.000083(16)
Largest diff. peak and hole	0.757 and -0.731 e. $Å^{-3}$
CCDC deposit	1832269

Table S2: Crystal data for **2.**

Empirical formula	$C_{107}\ H_{76}\ Cu_4\ N_{16}\ O_4$	
Formula weight	1903.99	
Temperature	150(2) K	
Wavelength	1.54178 Å	
Crystal system	Monoclinic	
Space group	P_n	
Unit cell dimensions	a = 12.9706(5) Å	α = 90°
	b = 14.3052(6) Å	β = 102.304(3)°
	c = 24.5777(9) Å	γ = 90°
Volume	4455.6(3) $Å^3$	
Z	2	
Density (calculated)	1.419 Mg/m^3	
Absorption coefficient	1.595 mm^{-1}	
F(000)	1956	
Crystal size	0.080 x 0.010 x 0.005 mm^3	
Theta range for data collection	3.089 to 67.253∞.	
Index ranges	-15<=h<=15, -17<=k<=16, -29<=l<=29	
Reflections collected	64940	
Independent reflections	15507 [R(int) = 0.1841]	
Completeness to theta = 67.253°	98.6 %	
Absorption correction	Semi-empirical from equivalents	
Max. and min. transmission	0.7529 and 0.6384	
Refinement method	Full-matrix least-squares on F^2	
Data / restraints / parameters	15507 / 2 / 1143	
Goodness-of-fit on F^2	1.028	
Final R indices [I>2sigma(I)]	R1 = 0.0697, wR2 = 0.1595	

R indices (all data)	R1 = 0.1398, wR2 = 0.2018
Absolute structure parameter	0.01(4)
Extinction coefficient	0.00081(13)
Largest diff. peak and hole	0.503 and -0.550 e. $Å^{-3}$
CCDC deposit	1832268

Table S3. Relevant bond distances (Å) and angles (°) for **1**.

Cu(1)-N(1)	1.905(4)
Cu(1)-O(1)	1.950(4)
Cu(1)-N(2)	1.960(5)
Cu(1)-O(2)	1.973(3)
Cu(2)-N(9)	1.899(4)
Cu(2)-O(1)	1.957(3)
Cu(2)-O(3)	1.973(3)
Cu(2)-N(10)	1.976(4)
Cu(3)-N(13)	1.904(4)
Cu(3)-O(3)	1.949(3)
Cu(3)-O(4)	1.958(4)
Cu(3)-N(14)	1.958(5)
Cu(4)-N(5)	1.892(4)
Cu(4)-O(4)	1.951(3)
Cu(4)-N(6)	1.970(4)
Cu(4)-O(2)	1.970(4)
O(1)-C(1)	1.359(6)
O(2)-C(29)	1.381(6)
O(3)-C(57)	1.357(6)
O(4)-C(85)	1.354(6)
N(1)-C(11)	1.370(6)
N(1)-C(2)	1.383(7)
N(2)-C(18)	1.307(7)
N(2)-C(19)	1.380(7)
N(3)-C(20)	1.395(6)

N(3)-C(6)	1.461(6)
N(4)-C(27)	1.315(7)
N(4)-C(28)	1.340(7)
N(5)-C(39)	1.371(7)
N(5)-C(30)	1.392(7)
N(6)-C(46)	1.319(7)
N(6)-C(47)	1.378(6)
N(7)-C(48)	1.405(8)
N(7)-C(34)	1.438(7)
N(8)-C(55)	1.313(8)
N(8)-C(56)	1.357(9)
N(9)-C(67)	1.375(6)
N(9)-C(58)	1.379(7)
N(10)-C(74)	1.330(7)
N(10)-C(75)	1.362(6)
N(11)-C(76)	1.402(7)
N(11)-C(62)	1.454(6)
N(12)-C(83)	1.338(7)
N(12)-C(84)	1.360(8)
N(13)-C(95)	1.356(6)
N(13)-C(86)	1.376(7)
N(14)-C(102)	1.324(7)
N(14)-C(103)	1.375(6)
N(15)-C(104)	1.399(7)
N(15)-C(90)	1.440(6)
N(16)-C(111)	1.316(7)
N(16)-C(112)	1.351(8)

N(1)-Cu(1)-O(1)	84.14(16)
N(1)-Cu(1)-N(2)	83.20(18)
O(1)-Cu(1)-N(2)	164.99(17)
N(1)-Cu(1)-O(2)	175.72(17)
O(1)-Cu(1)-O(2)	91.64(15)
N(2)-Cu(1)-O(2)	100.88(17)
N(9)-Cu(2)-O(1)	175.28(16)
N(9)-Cu(2)-O(3)	83.58(15)

O(1)-Cu(2)-O(3)	91.83(14)
N(9)-Cu(2)-N(10)	83.53(18)
O(1)-Cu(2)-N(10)	100.77(17)
O(3)-Cu(2)-N(10)	163.39(16)
N(13)-Cu(3)-O(3)	172.22(18)
N(13)-Cu(3)-O(4)	84.11(16)
O(3)-Cu(3)-O(4)	91.60(15)
N(13)-Cu(3)-N(14)	83.48(18)
O(3)-Cu(3)-N(14)	100.09(17)
O(4)-Cu(3)-N(14)	166.47(16)
N(5)-Cu(4)-O(4)	177.00(18)
N(5)-Cu(4)-N(6)	83.50(19)
O(4)-Cu(4)-N(6)	99.45(16)
N(5)-Cu(4)-O(2)	84.10(16)
O(4)-Cu(4)-O(2)	93.05(14)
N(6)-Cu(4)-O(2)	164.90(16)
C(1)-O(1)-Cu(1)	111.1(3)
C(1)-O(1)-Cu(2)	117.2(3)
Cu(1)-O(1)-Cu(2)	125.19(19)
C(29)-O(2)-Cu(4)	110.3(3)
C(29)-O(2)-Cu(1)	116.9(3)
Cu(4)-O(2)-Cu(1)	127.12(18)
C(57)-O(3)-Cu(3)	118.7(3)
C(57)-O(3)-Cu(2)	110.5(3)
Cu(3)-O(3)-Cu(2)	126.47(19)
C(85)-O(4)-Cu(4)	120.2(3)
C(85)-O(4)-Cu(3)	110.7(3)
Cu(4)-O(4)-Cu(3)	120.34(18)
C(11)-N(1)-C(2)	129.4(4)
C(11)-N(1)-Cu(1)	115.6(4)
C(2)-N(1)-Cu(1)	114.9(3)
C(18)-N(2)-C(19)	119.7(5)
C(18)-N(2)-Cu(1)	128.1(4)
C(19)-N(2)-Cu(1)	112.0(4)
C(20)-N(3)-C(6)	119.3(4)
C(27)-N(4)-C(28)	117.2(5)

C(39)-N(5)-C(30)	129.5(5)
C(39)-N(5)-Cu(4)	115.4(4)
C(30)-N(5)-Cu(4)	114.9(3)
C(46)-N(6)-C(47)	120.0(5)
C(46)-N(6)-Cu(4)	129.1(4)
C(47)-N(6)-Cu(4)	110.9(4)
C(48)-N(7)-C(34)	117.9(5)
C(55)-N(8)-C(56)	116.9(6)
C(67)-N(9)-C(58)	129.4(4)
C(67)-N(9)-Cu(2)	115.5(4)
C(58)-N(9)-Cu(2)	115.1(3)
C(74)-N(10)-C(75)	120.6(5)
C(74)-N(10)-Cu(2)	128.4(4)
C(75)-N(10)-Cu(2)	111.0(4)
C(76)-N(11)-C(62)	117.9(4)
C(83)-N(12)-C(84)	116.8(6)
C(95)-N(13)-C(86)	130.1(4)
C(95)-N(13)-Cu(3)	115.6(4)
C(86)-N(13)-Cu(3)	114.2(3)
C(102)-N(14)-C(103)	119.4(5)
C(102)-N(14)-Cu(3)	129.1(3)
C(103)-N(14)-Cu(3)	111.4(4)
C(104)-N(15)-C(90)	121.2(5)
C(111)-N(16)-C(112)	116.5(5)
O(1)-C(1)-C(6)	123.5(4)
O(1)-C(1)-C(2)	117.7(5)

Table S4. Relevant bond distances (Å) and angles (°) for **2**.

Cu(1)-N(1)	1.900(10)
Cu(1)-O(2)	1.920(8)
Cu(1)-N(2)	1.950(11)
Cu(1)-O(1)	1.970(8)
Cu(2)-N(9)	1.892(11)
Cu(2)-O(3)	1.963(9)
Cu(2)-O(1)	1.967(9)
Cu(2)-N(10)	1.984(11)
Cu(3)-N(13)	1.901(10)
Cu(3)-O(4)	1.943(9)
Cu(3)-O(3)	1.945(8)
Cu(3)-N(14)	1.956(10)
Cu(3)-N(11)	2.401(11)
Cu(4)-N(5)	1.889(11)
Cu(4)-O(2)	1.965(9)
Cu(4)-N(6)	1.968(12)
Cu(4)-O(4)	1.974(9)
O(1)-C(1)	1.392(16)
O(2)-C(26)	1.342(16)
O(3)-C(51)	1.356(15)
O(4)-C(76)	1.340(16)
N(1)-C(8)	1.355(17)
N(1)-C(2)	1.395(16)
N(2)-C(15)	1.341(17)
N(2)-C(16)	1.382(16)
N(3)-C(6)	1.416(17)
N(3)-C(17)	1.435(19)
N(4)-C(24)	1.308(19)
N(4)-C(25)	1.39(2)
N(5)-C(33)	1.365(18)
N(5)-C(27)	1.387(17)

N(6)-C(40)	1.335(18)
N(6)-C(41)	1.371(17)
N(7)-C(42)	1.406(18)
N(7)-C(31)	1.442(16)
N(8)-C(49)	1.34(2)
N(8)-C(50)	1.377(19)
N(9)-C(58)	1.359(16)
N(9)-C(52)	1.387(17)
N(10)-C(65)	1.312(17)
N(10)-C(66)	1.361(16)
N(11)-C(67)	1.392(16)
N(11)-C(56)	1.465(16)
N(12)-C(74)	1.335(19)
N(12)-C(75)	1.410(19)
N(13)-C(83)	1.367(16)
N(13)-C(77)	1.417(16)
N(14)-C(90)	1.339(18)
N(14)-C(91)	1.355(17)
N(15)-C(92)	1.401(16)
N(15)-C(81)	1.437(17)
N(16)-C(99)	1.330(18)
N(16)-C(100)	1.366(17)

N(1)-Cu(1)-O(2)	164.7(4)
N(1)-Cu(1)-N(2)	83.5(5)
O(2)-Cu(1)-N(2)	97.2(4)
N(1)-Cu(1)-O(1)	85.0(4)
O(2)-Cu(1)-O(1)	95.0(4)
N(2)-Cu(1)-O(1)	167.8(4)
N(9)-Cu(2)-O(3)	83.9(4)
N(9)-Cu(2)-O(1)	174.8(4)
O(3)-Cu(2)-O(1)	91.7(4)
N(9)-Cu(2)-N(10)	83.3(5)
O(3)-Cu(2)-N(10)	166.5(4)
O(1)-Cu(2)-N(10)	100.8(4)
N(13)-Cu(3)-O(4)	84.2(4)

N(13)-Cu(3)-O(3)	171.2(4)
O(4)-Cu(3)-O(3)	91.7(3)
N(13)-Cu(3)-N(14)	83.3(4)
O(4)-Cu(3)-N(14)	167.5(4)
O(3)-Cu(3)-N(14)	100.5(4)
N(13)-Cu(3)-N(11)	107.7(4)
O(4)-Cu(3)-N(11)	89.5(4)
O(3)-Cu(3)-N(11)	80.0(4)
N(14)-Cu(3)-N(11)	95.3(4)
N(5)-Cu(4)-O(2)	83.9(4)
N(5)-Cu(4)-N(6)	83.4(5)
O(2)-Cu(4)-N(6)	166.0(4)
N(5)-Cu(4)-O(4)	156.7(4)
O(2)-Cu(4)-O(4)	93.0(4)
N(6)-Cu(4)-O(4)	101.0(4)
C(1)-O(1)-Cu(2)	114.9(8)
C(1)-O(1)-Cu(1)	108.8(8)
Cu(2)-O(1)-Cu(1)	126.5(4)
C(26)-O(2)-Cu(1)	122.1(8)
C(26)-O(2)-Cu(4)	110.9(8)
Cu(1)-O(2)-Cu(4)	117.2(4)
C(51)-O(3)-Cu(3)	117.9(8)
C(51)-O(3)-Cu(2)	110.7(8)
Cu(3)-O(3)-Cu(2)	130.8(5)
C(76)-O(4)-Cu(3)	111.5(8)
C(76)-O(4)-Cu(4)	123.7(8)
Cu(3)-O(4)-Cu(4)	124.7(4)
C(8)-N(1)-C(2)	129.9(11)
C(8)-N(1)-Cu(1)	115.9(9)
C(2)-N(1)-Cu(1)	113.6(8)
C(15)-N(2)-C(16)	118.6(11)
C(15)-N(2)-Cu(1)	129.5(9)
C(16)-N(2)-Cu(1)	111.9(8)
C(6)-N(3)-C(17)	119.3(12)
C(24)-N(4)-C(25)	118.5(15)
C(33)-N(5)-C(27)	128.6(12)

C(33)-N(5)-Cu(4)	115.9(9)
C(27)-N(5)-Cu(4)	115.5(8)
C(40)-N(6)-C(41)	120.3(13)
C(40)-N(6)-Cu(4)	129.4(10)
C(41)-N(6)-Cu(4)	110.0(9)
C(42)-N(7)-C(31)	116.3(11)
C(49)-N(8)-C(50)	117.5(14)
C(58)-N(9)-C(52)	128.0(11)
C(58)-N(9)-Cu(2)	116.5(9)
C(52)-N(9)-Cu(2)	115.4(8)
C(65)-N(10)-C(66)	120.7(12)
C(65)-N(10)-Cu(2)	128.6(10)
C(66)-N(10)-Cu(2)	110.4(9)
C(67)-N(11)-C(56)	119.8(11)
C(67)-N(11)-Cu(3)	116.0(8)
C(56)-N(11)-Cu(3)	101.8(8)
C(74)-N(12)-C(75)	115.1(13)
C(83)-N(13)-C(77)	130.3(11)
C(83)-N(13)-Cu(3)	115.4(8)
C(77)-N(13)-Cu(3)	114.2(8)
C(90)-N(14)-C(91)	119.3(12)
C(90)-N(14)-Cu(3)	128.4(10)
C(91)-N(14)-Cu(3)	112.2(9)
C(92)-N(15)-C(81)	120.1(11)
C(99)-N(16)-C(100)	115.7(12)

Figure S1. Molecular structure of **2** (displacement ellipsoids at 30% probability). H atoms and solvent molecules removed for clarity. Bond distances and angles can be found in Table S4. CCDC: 1832268

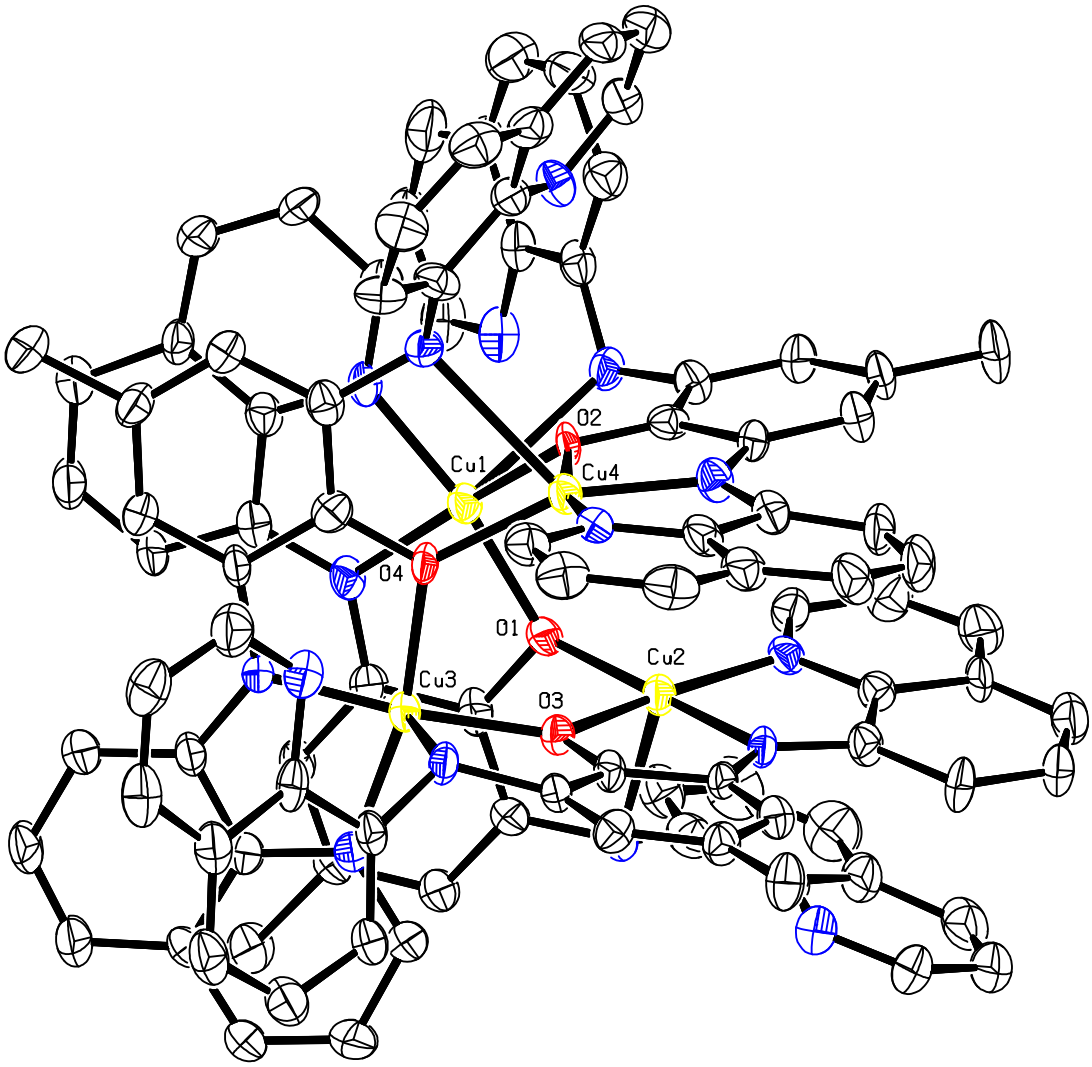

Figure S2. View of the molecular structure of **2** highlighting the Cu_4O_4 core and the long axial Cu-N coordinate bonds from the rotated aminoquinolyl substituent. H atoms and solvent omitted for clarity.

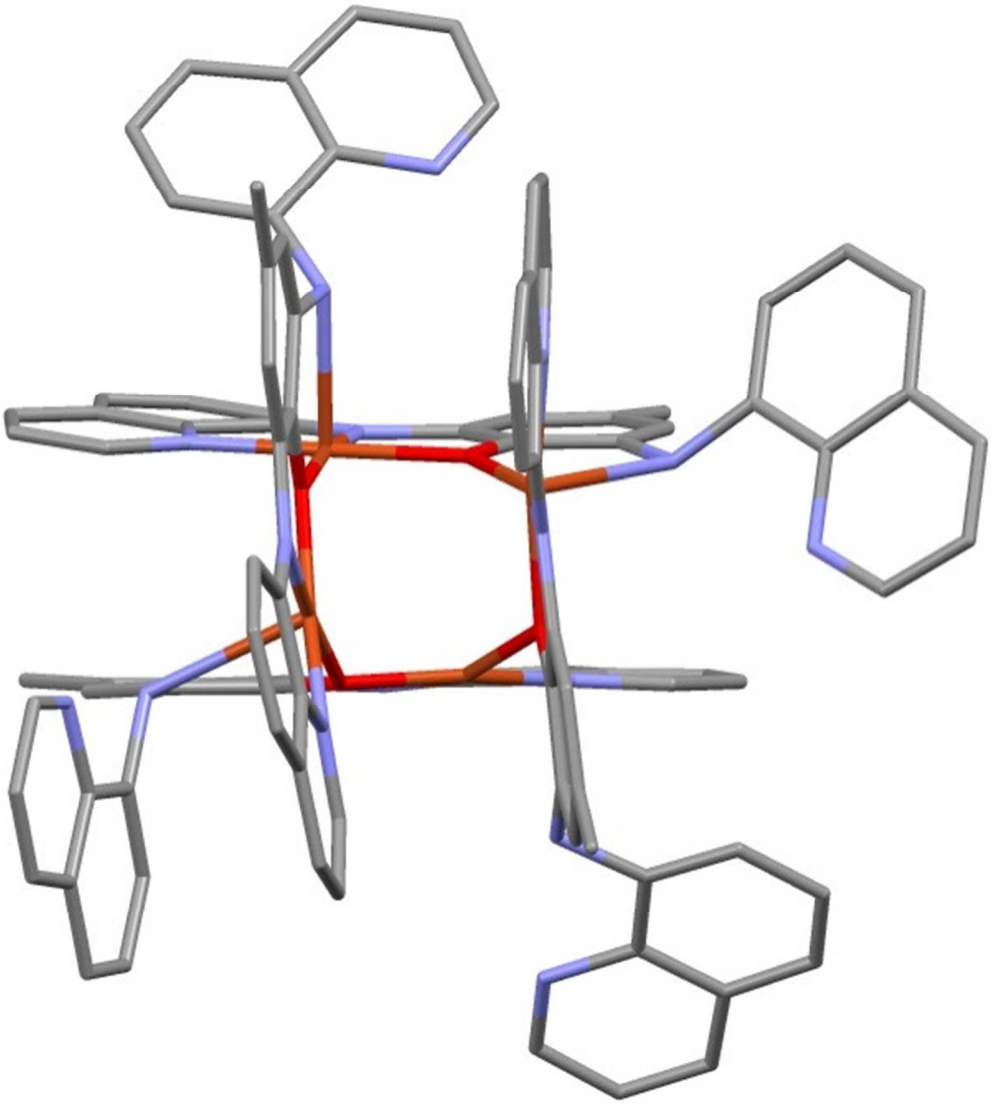

Figure S3. View of the Cu_4O_4 core in **2**.

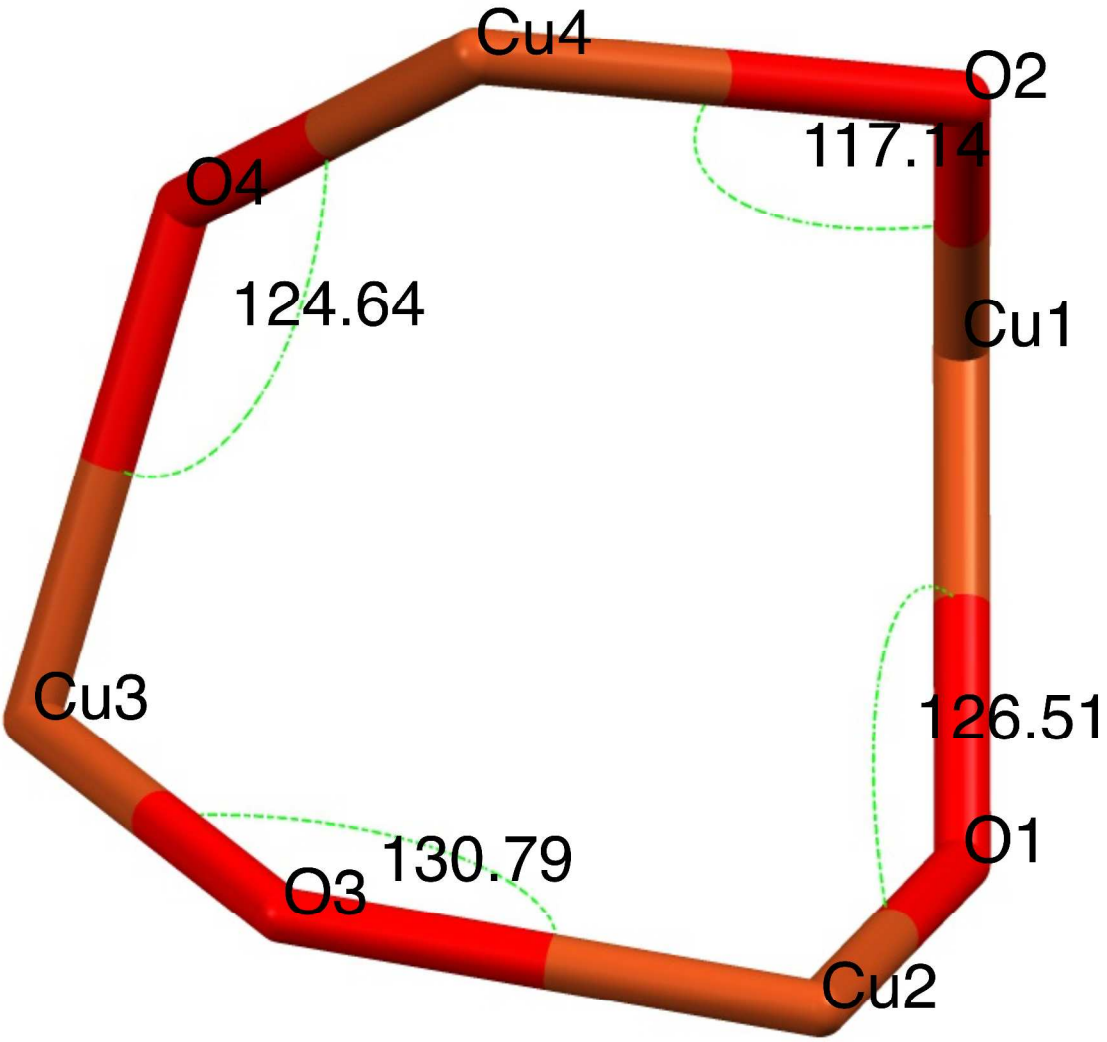

Figure S4. ^{1}H NMR spectrum of **4** in $CDCl_3$.

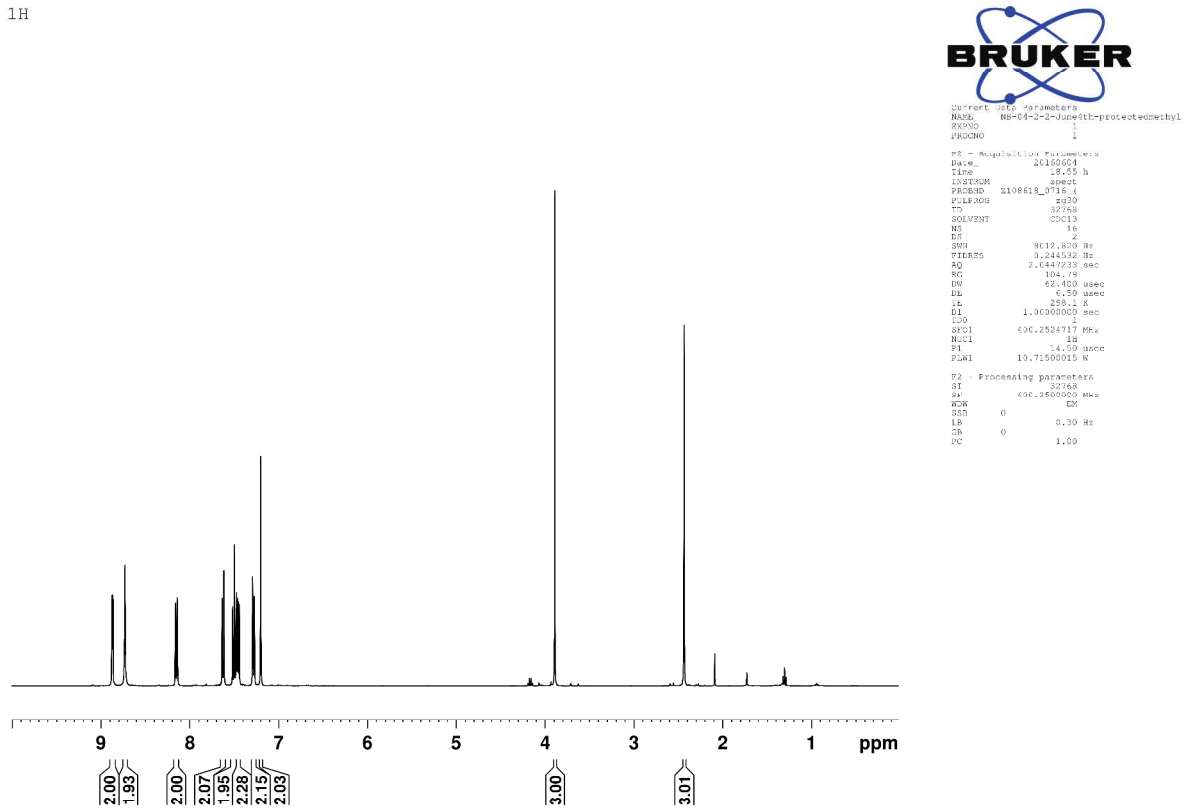

Figure S5. ^{13}C NMR spectrum of **4** in $CDCl_3$.

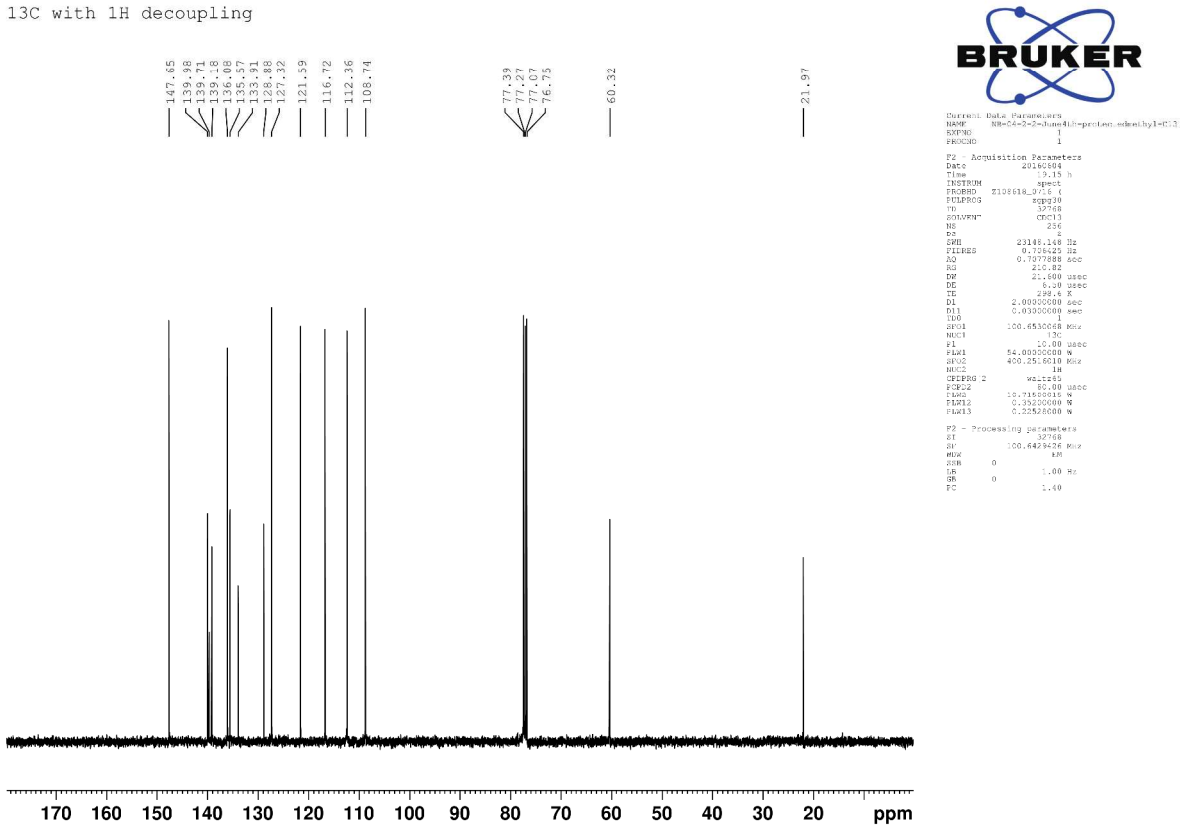

Figure S6. ESI mass spectrum of **1** in THF/MeOH with isotope distribution (experimental, top) and calculated (bottom) for $[M+H]^+$.

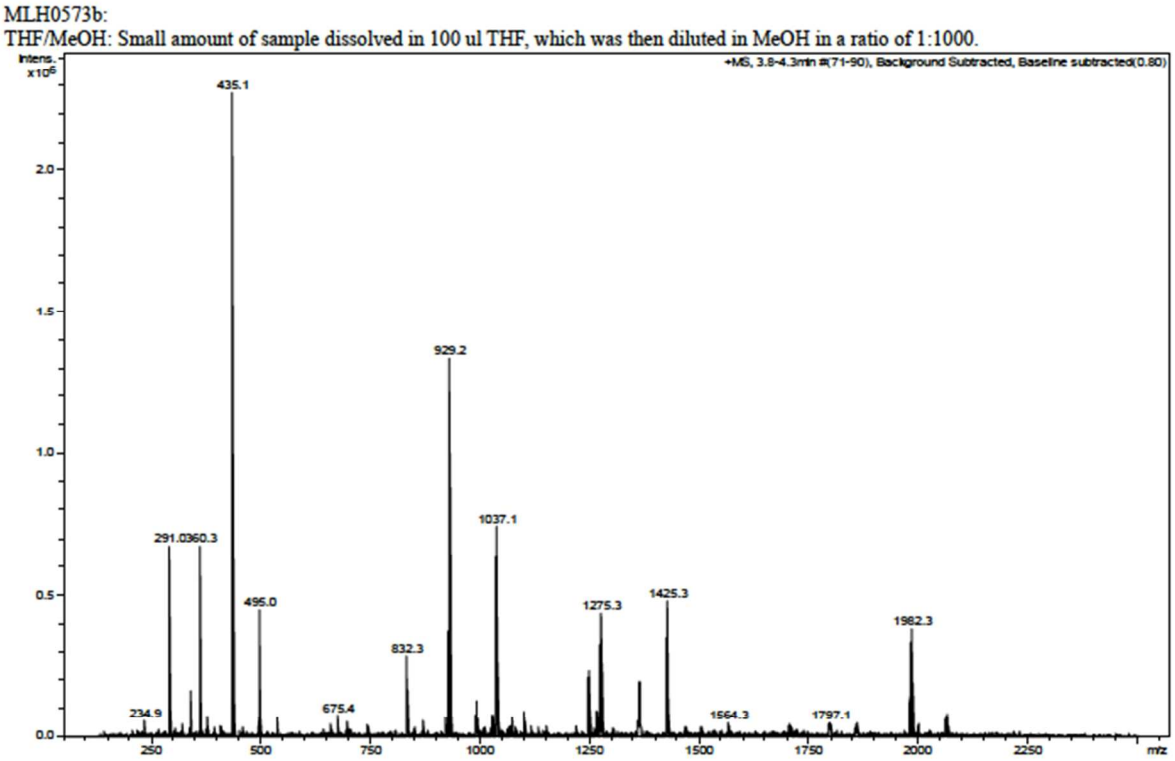

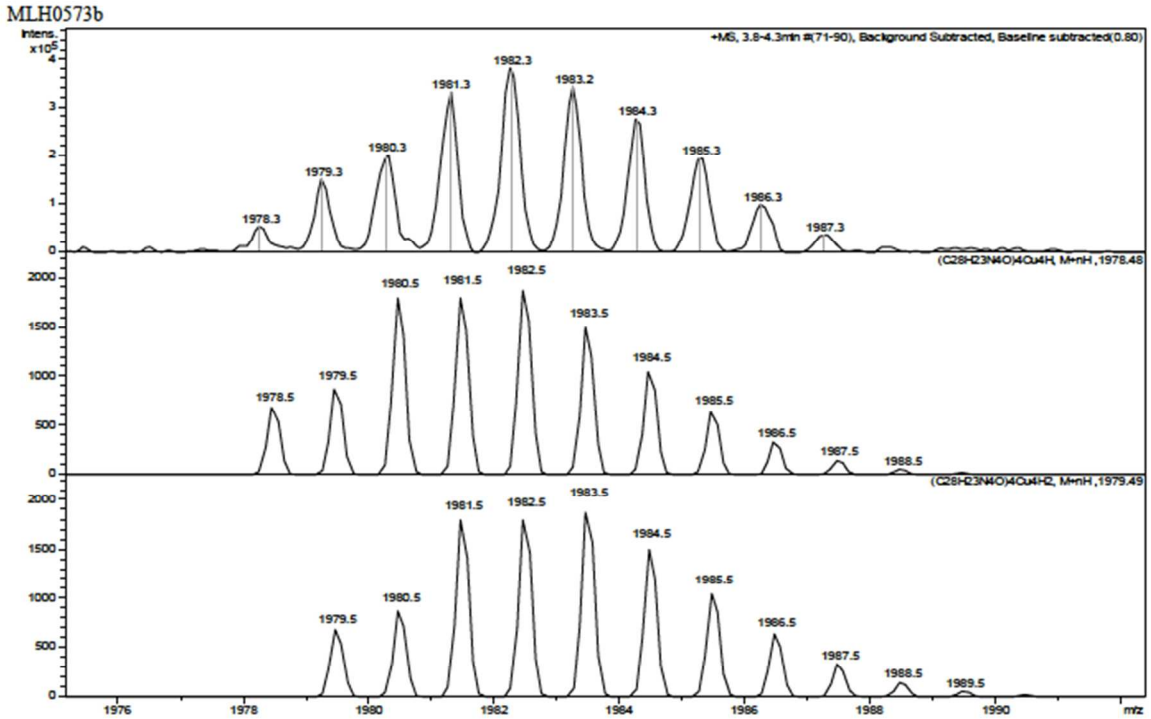

Figure S7. ESI mass spectrum of **2** in THF/MeOH with isotope distribution (experimental, top) and calculated (bottom) for $[M+4H]^+$.

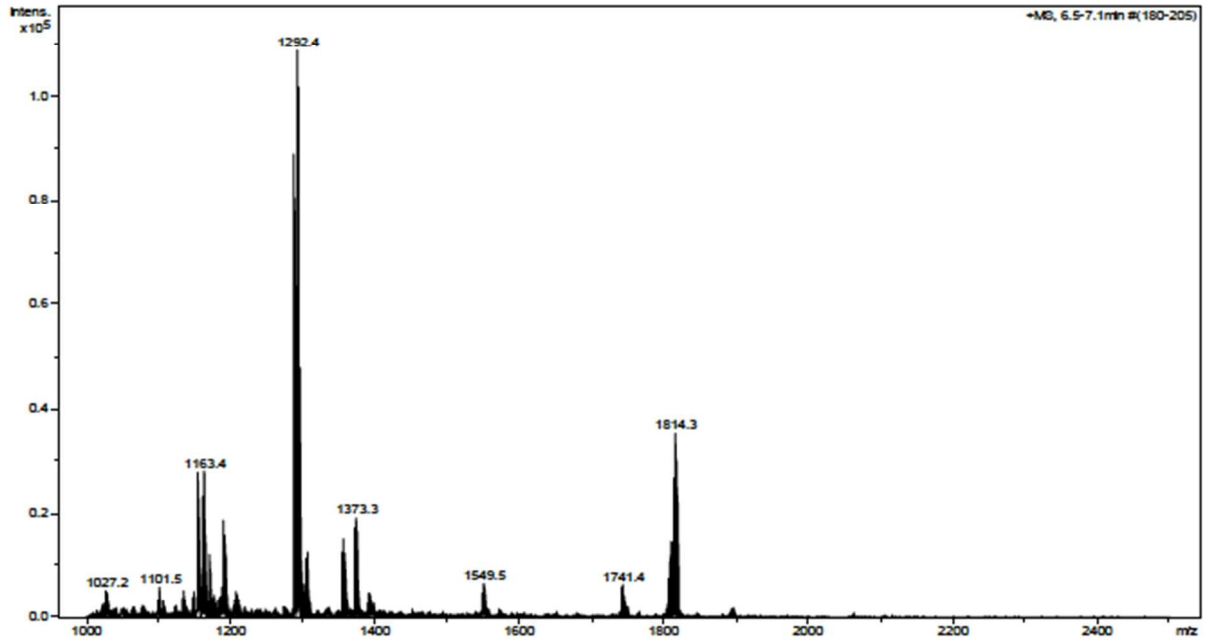

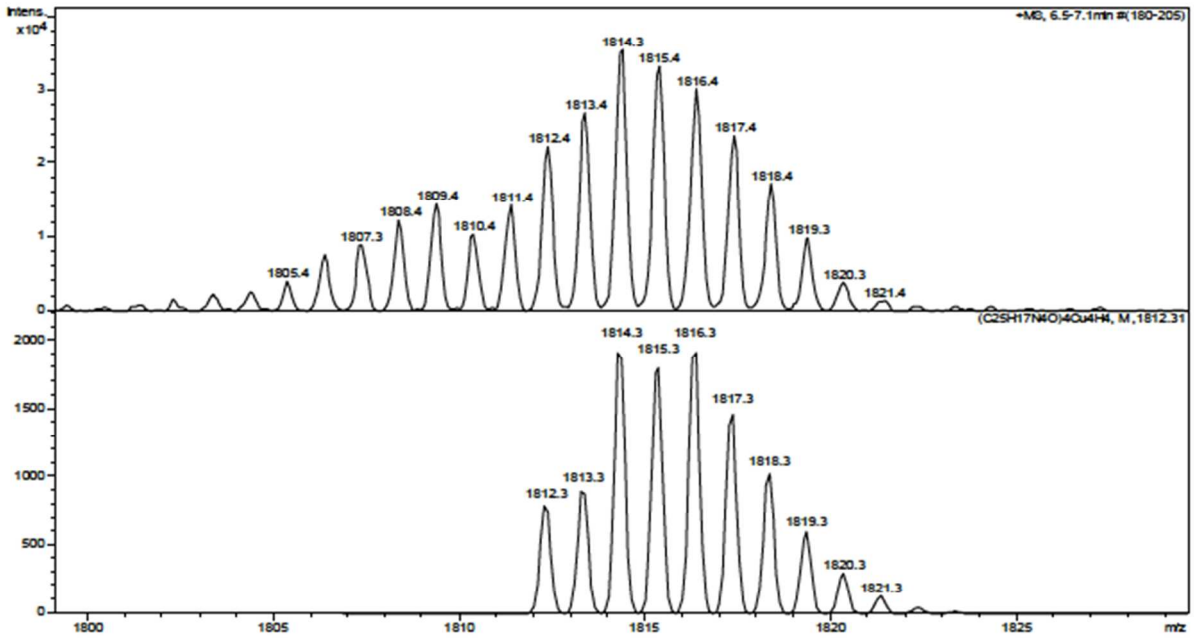

Figure S8. Comparison of the FT-IR spectra of powder and single crystal samples of **1**.

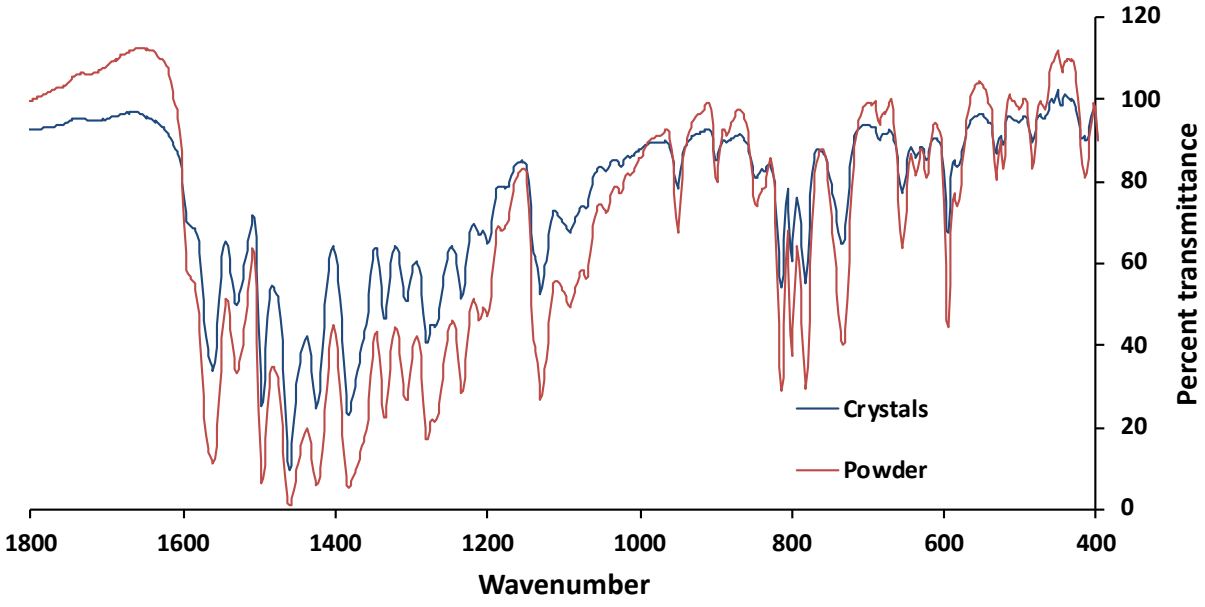

Figure S9. Comparison of the UV-visible spectra of powder and single crystal samples of **1** in CH_2Cl_2. Red trace is the single crystals and blue trace is from precipitated powder.

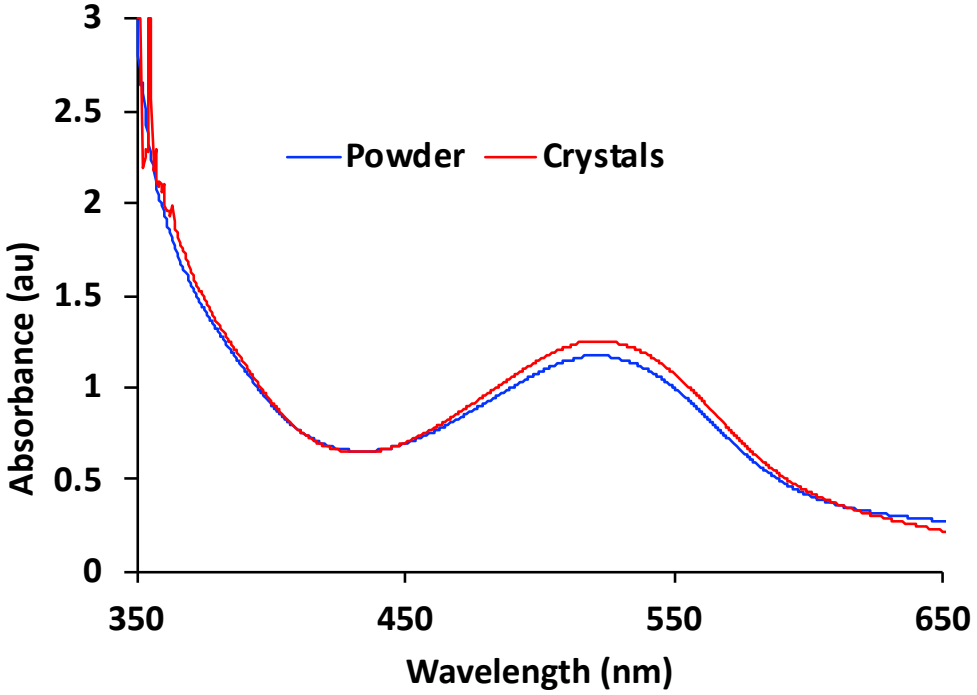

Figure S10. Experimental pXRD spectrum of complex **1**.

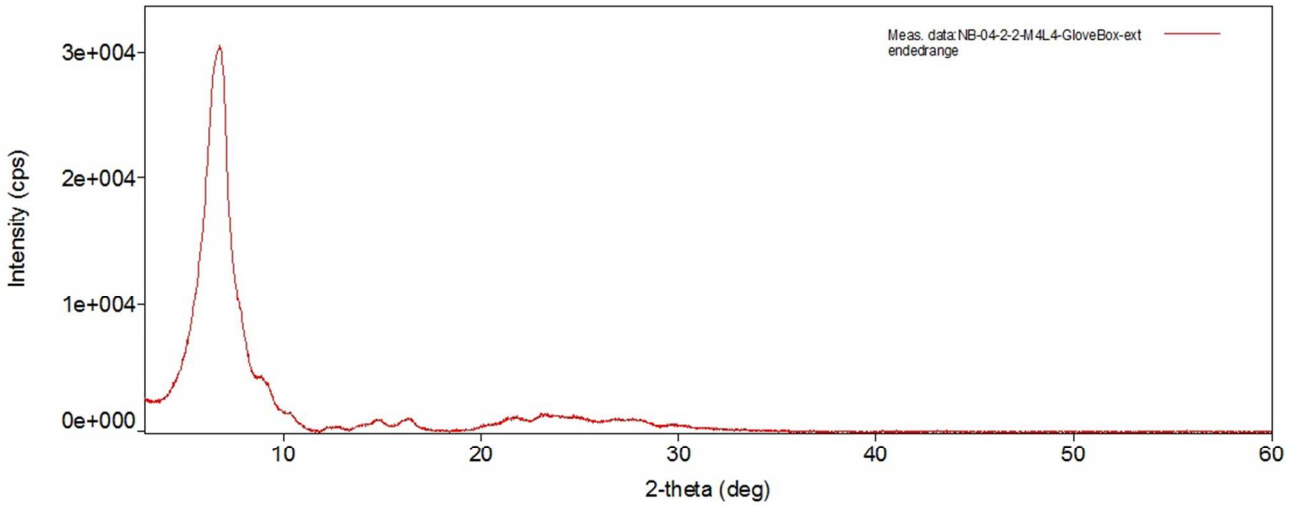

Figure S11. Calculated pXRD spectrum from the single crystal X-ray structure of **1**

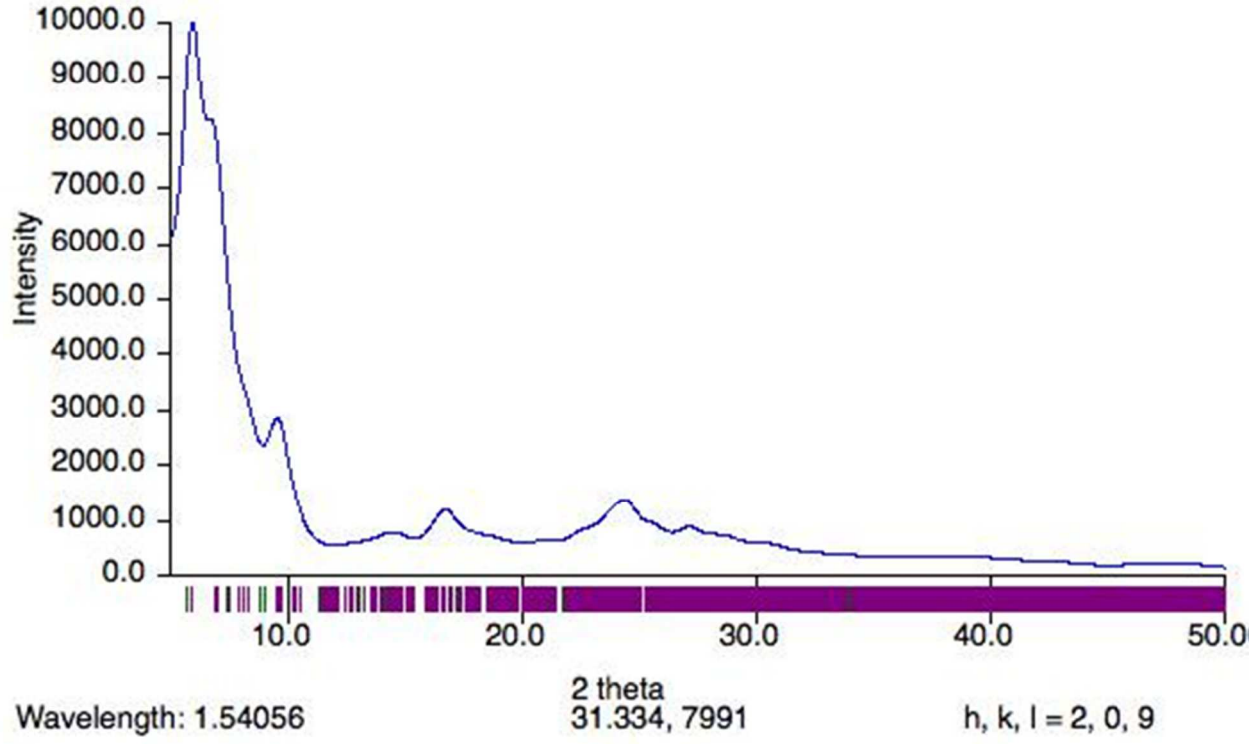

Figure S12. Experimental pXRD spectrum of complex **2**.

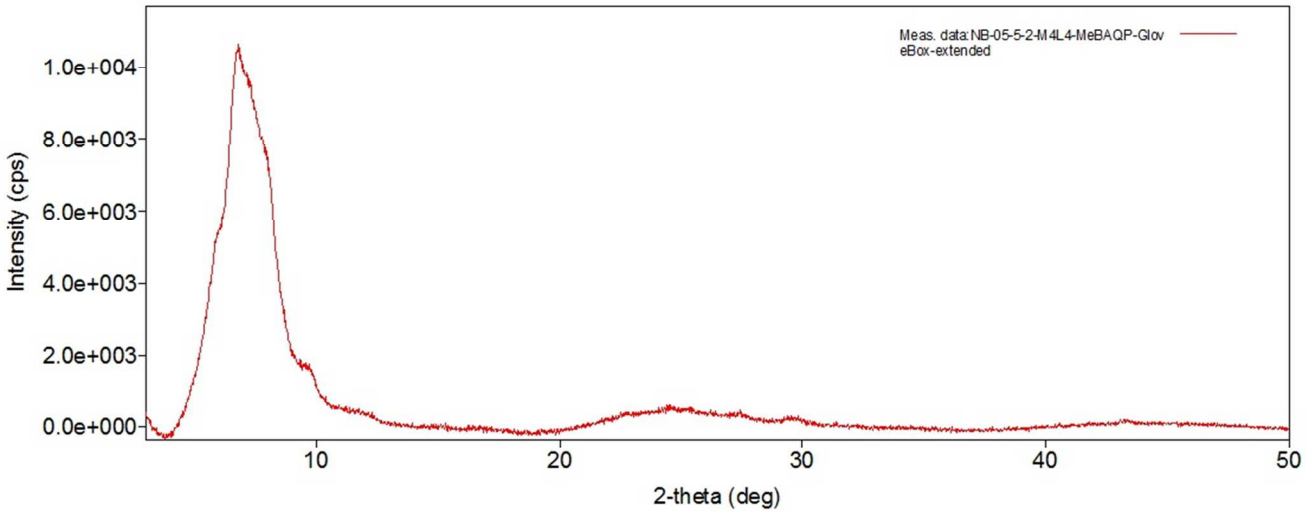

Figure S13. Calculated pXRD spectrum from the single crystal X-ray structure of **2.**

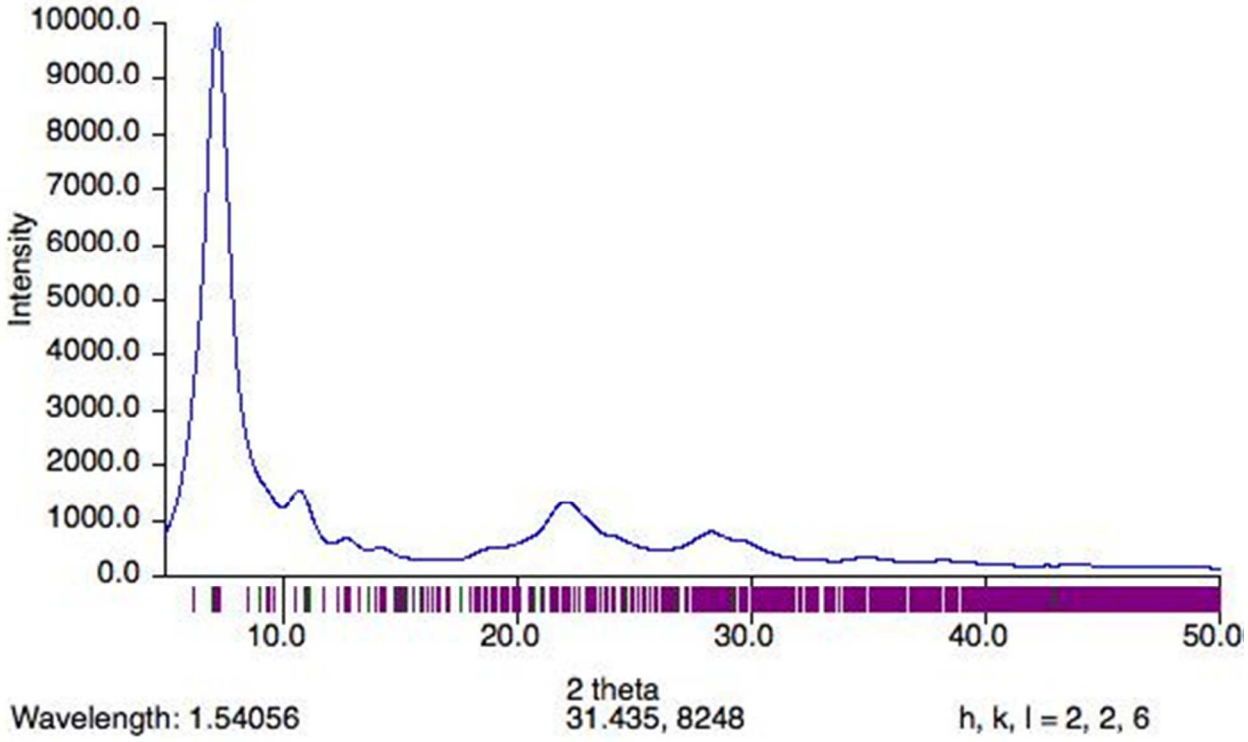

Figure S14. UV-visible-NIR spectrum of **1** (red trace) in THF at 300 K. Black trace (addition of 2 equiv $AgPF_6$). Blue trace (addition of 4 equiv $AgPF_6$). Beyond 4 equiv results in the decrease in the absorbance of the broad NIR absorptions.

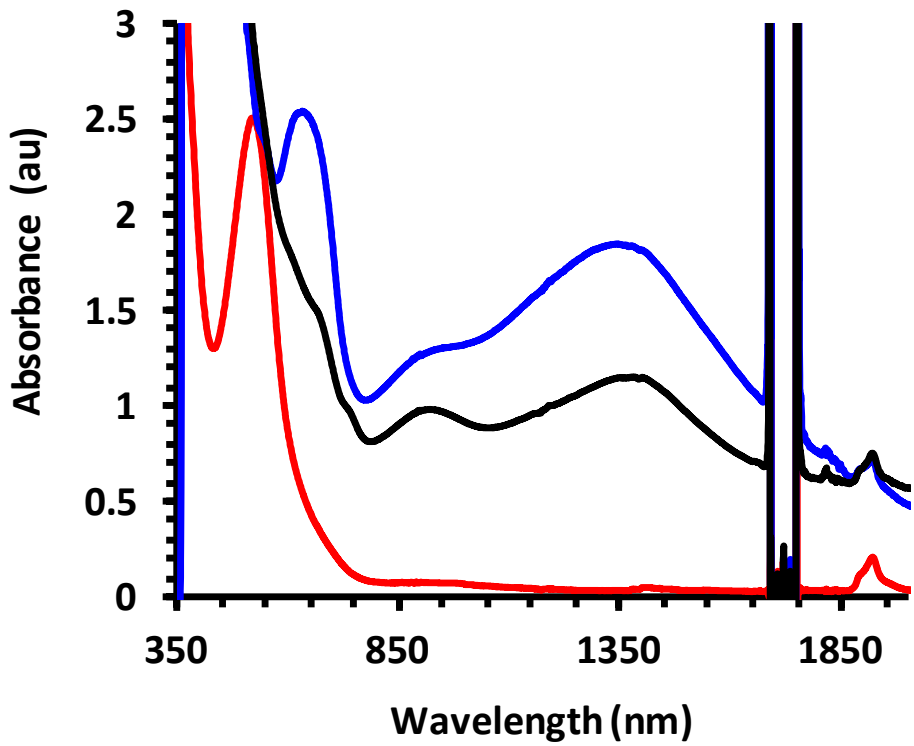

Figure S15. Magnetic exchange coupling model used in the fitting of **1** and **2** (including the spin Hamiltonian).

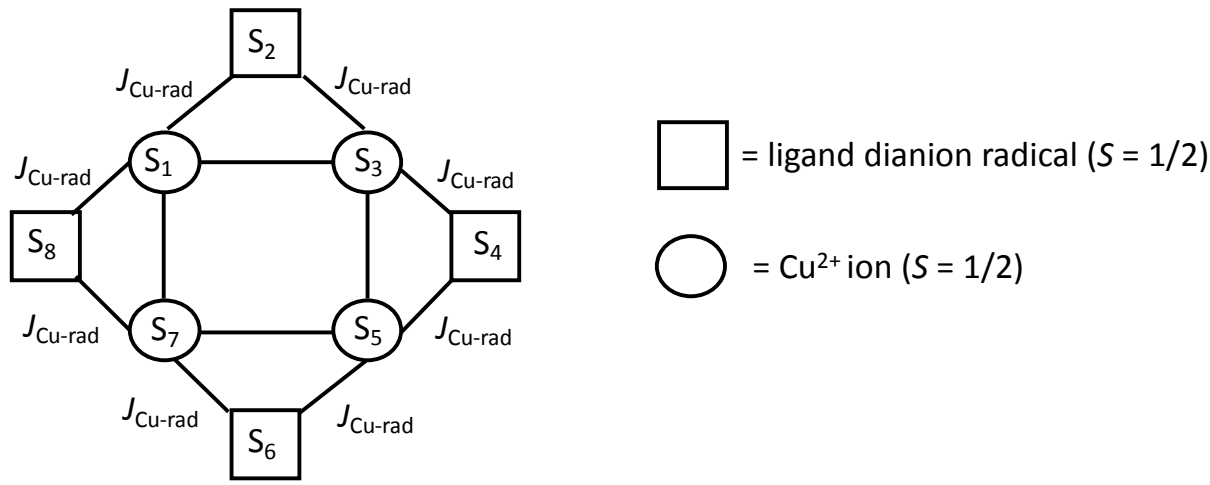

Spin Hamiltonian:

$$\hat{H} = -2J_{Cu-rad}\{\hat{S}_1 \cdot \hat{S}_2 + \hat{S}_2 \cdot \hat{S}_3 + \hat{S}_3 \cdot \hat{S}_4 + \hat{S}_4 \cdot \hat{S}_5 + \hat{S}_5 \cdot \hat{S}_6 + \hat{S}_6 \cdot \hat{S}_7 + \hat{S}_7 \cdot \hat{S}_8 + \hat{S}_8 \cdot \hat{S}_1\}$$

Figure S16. Variable temperature magnetic susceptibility data for **2** (external field 5000 Oe). Experimental data are red squares and black line represents the best fit to the experimental data. Top: Plot of $\chi_m T$ vs temperature. Bottom: Plot of χ_m vs temperature.

Best fit parameters: $J_{Cu\text{-}rad}$ = -97 cm^{-1}, g_{av} = 2.050, zJ' = -0.52 cm^{-1}, temperature independent paramagnetism (TIP) = 1.25 × 10^{-3} cm^3 mol^{-1}, ρ = 0.027, *Residual* = 0.010.

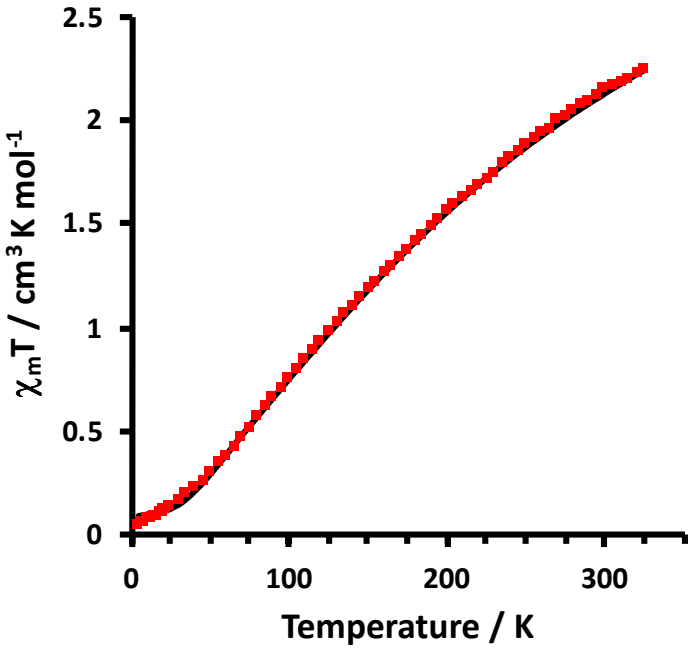

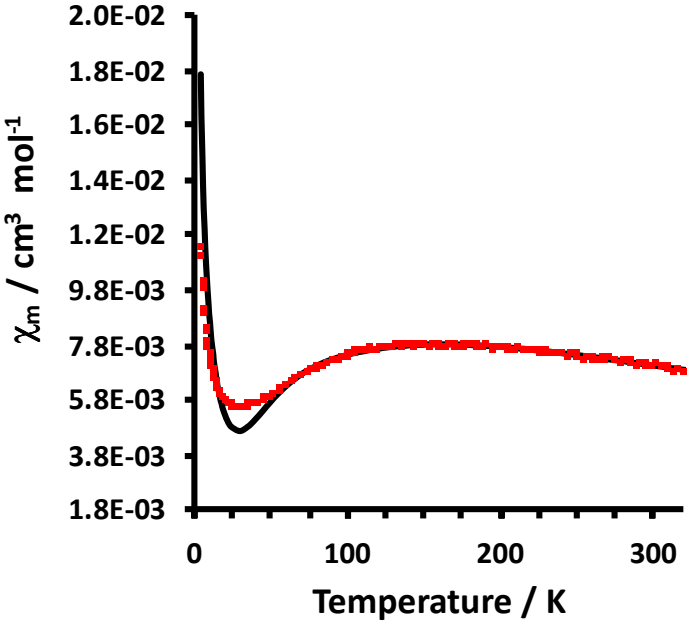

Figure S17. Mulliken spin densities in the unrestricted singlet state of complex **1** (B3LYP/def2-svp). Red is α and blue is β spin density. Isovalue 0.01.

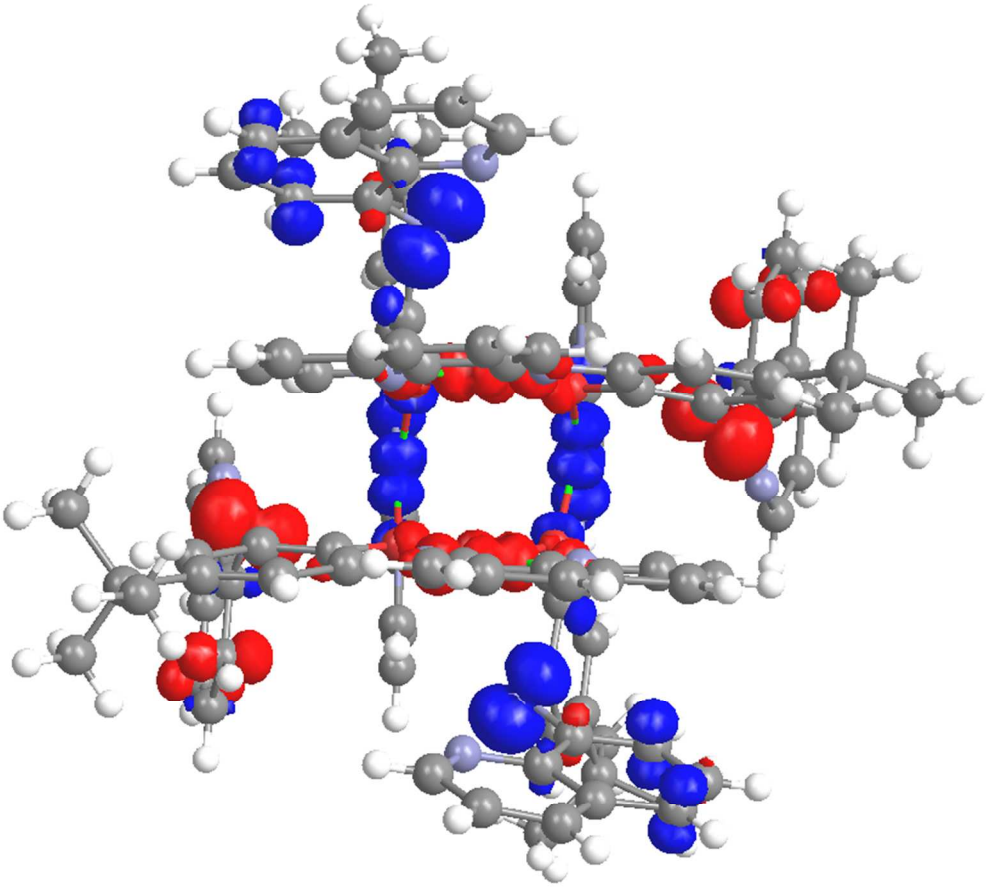

Table S5. Mulliken spin densities of selected atoms in complex **1.**

Atom	Spin density	Atom	Spin density
Cu1	0.60	N11	-0.62
Cu2	-0.60	N15	0.66
Cu3	0.60	O1	0.05
Cu4	-0.60	O2	-0.05
N3	0.63	O3	-0.05
N7	-0.66	O4	0.04

Figure S18. Mulliken spin densities in the unrestricted singlet state of complex **2** (B3LYP/def2-svp). Red is α and blue is β spin density. Isovalue 0.01.

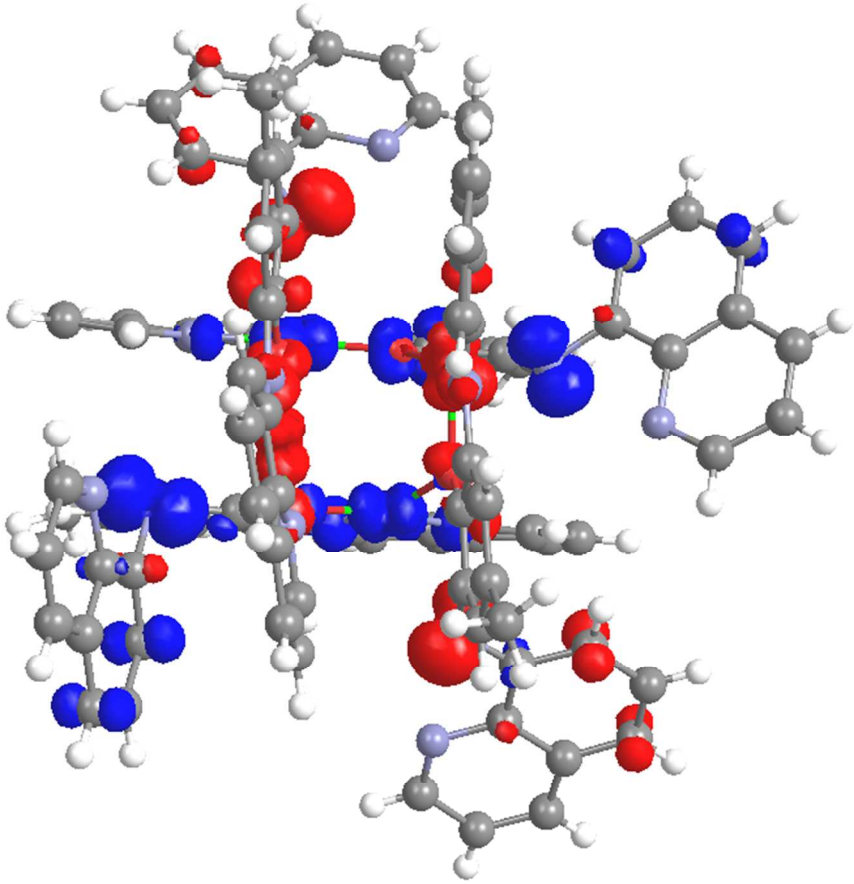

Table S6. Mulliken spin densities of selected atoms in complex **2.**

Atom	Spin density	Atom	Spin density
Cu1	-0.60	N11	0.59
Cu2	0.61	N15	-0.53
Cu3	-0.61	O1	-0.04
Cu4	0.61	O2	0.06
N3	-0.70	O3	0.08
N7	0.66	O4	-0.10